Audio-magnetotelluric survey of a shallow aquifer east of Mesa del Contadero, central New Mexico

Shari A. Kelley and Daniel J. Koning
2022, pp. 329-339. https://doi.org/10.56577/FFC-72.329

in:

Socorro Region III, Koning, Daniel J.; Hobbs, Kevin J.; Phillips, Fred M.; Nelson, W. John; Cather, Steven M.; Jakle, Anne C.; Van Der Werff, Brittney, New Mexico Geological Society 72nd Annual Fall Field Conference Guidebook, 426 p. https://doi.org/10.56577/FFC-72

This page is intentionally left blank to maintain order of facing pages.

New Mexico Geological Society Guidebook, 72nd Fall Field Conference, 2022, p. 329–339.

AUDIO-MAGNETOTELLURIC SURVEY OF A SHALLOW AQUIFER EAST OF MESA DEL CONTADERO, CENTRAL NEW MEXICO

SHARI A. KELLEY[1] AND DANIEL J. KONING[1]

[1]New Mexico Bureau of Geology and Mineral Resources, New Mexico Institute of Mining and Technology, 801 Leroy Place, Socorro, NM 87801; shari.kelley@nmt.edu

Abstract—The subsurface hydrogeology in the vicinity of Mesa Camp on the Armendaris Ranch in central New Mexico was investigated using the audio-magnetotelluric (AMT) geophysical method. Data were collected at two sites about 1 km from the camp. One-dimensional modeling of the data revealed a shallow resistive layer between the land surface and depths of 70–90 m below the land surface, a shallow conductor with a base at 100–130 m, and a deeper resistive and conductive pair below depths of 130 m. The shallow resistive layer corresponds to the vadose zone in the axial Rio Grande facies of the Sierra Ladrones aquifer. By combining the AMT data with information derived from recent geologic mapping in the area and limited drillhole logs, we present three geologically reasonable scenarios for the subsurface hydrogeology beneath Mesa Camp.

INTRODUCTION

The productivity of a water well at Mesa Camp, a remote bunkhouse on the Armendaris Ranch near Mesa del Contadero in central New Mexico (Figs. 1 and 2), has declined over the years. The well, which was drilled to a depth of 94 m, yielded 30 gpm in the year of 1969, then 15 gpm in the year 1975, and is now down to 2.4 gpm. According to the owners, no other information about the well is available, and no well record was found on the Office of the State Engineer website. In trying to decide whether to simply deepen the existing well or drill a new well, the landowner asked for information about the subsurface geology and potential aquifers or aquitards. To learn more about the local hydrogeology of the basin, we collected audio-magnetotelluric (AMT) data at two sites (MC01 and MC02) near Mesa Camp (Figs. 1 and 2). The AMT method is well suited for measuring the resistivity structure of the subsurface to depths of 1.5 km, which is the maximum depth range of most water wells; these measurements can then be used to infer hydrogeologic structure. This preliminary AMT investigation supplements ongoing geological and geophysical (gravity survey) research in this area that is intended to better constrain complex stratigraphy and structures in the transition between two Rio Grande rift basins: the Socorro Basin to the north and the San Marcial Basin to the south (Figs. 1 and 2; Koning et al., 2020 a, b, 2021a, b; Gallant et al., this volume).

HYDROGEOLOGIC SETTING

Structure

The study area (Figs. 1 and 2) lies in a poorly defined boundary zone between the Socorro and San Marcial basins. Two major faults project into the area from the northeast and southwest. The fault to the northeast is the Little San Pascual Mountains fault zone (*sensu* Jochems and Love, 2016), which has three northeast-striking strands (Koning et al., 2020a, 2021a). The total width of the fault zone is about 2.0–2.5 km. This fault zone has down-to-the-northwest normal offset, with throws of ~1 km for the east strand and at least several hundred meters for the west and central strands (Koning and Heizler, this volume). The fault strands are well defined near the Little San Pascual Mountains but cannot be mapped with confidence south of these mountains (Koning et al., 2020a, b, 2021a). To the southeast, a pronounced northeast-striking, northwest-down gradient in Bouguer anomaly data supports the interpretation of a west-down, northeast-striking fault zone called the Lava fault zone (Gallant et al., this volume; Fig. 1). A notable gravity gradient 0.5 km north of Mesa Camp was used to extend the west strand of the Little San Pascual Mountain fault southwards to the general area where the AMT data were collected (Fig. 2).

Stratigraphy

The complete stratigraphy of the Socorro region is illustrated inside the back cover of this guidebook. West of and beneath the Socorro Basin, the Mesozoic and Permian section has been removed during exhumation of a Laramide uplift (i.e., the Sierra uplift; Cather, 1983; Koning et al., this volume). Within this stratigraphy the axial facies of the Palomas Formation is a common aquifer in this region (Koning et al., this volume). The distal playa facies of the Popotosa Formation, Cretaceous shales, and mud-rich units in the Abo Formation act as aquitards.

The nearest bedrock exposures are in the Little San Pascual Mountains (7–12 km to the northeast, on the Sierra uplift), in the southernmost Chupadera Mountains (10 km to the northwest, also on the Sierra uplift), and the northern Fra Cristobal Mountains (21 km to the southwest). The Little San Pascual Mountains contain a complete, conformable sequence of Pennsylvanian, limestone-rich strata overlain by Permian strata, the latter containing (in ascending order) the Bursum, Abo, Yeso, Glorieta, and San Andres formations (Koning et al.,

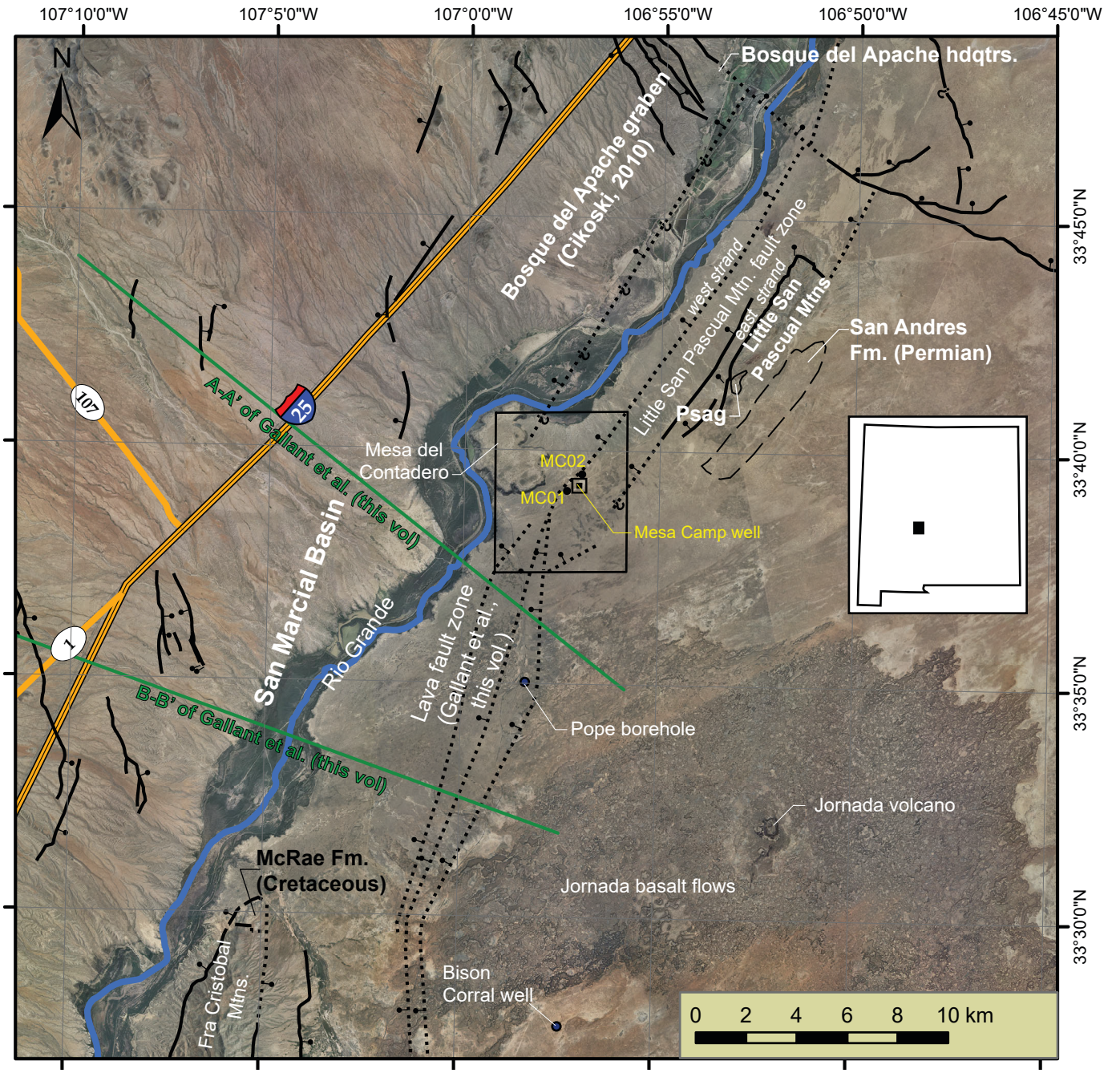

FIGURE 1. Location map for the study area. Black rectangle outlines the area of Figure 2. The basalt-capped Mesa del Contadero is located 1.6 km to the northwest of Mesa Camp. The study area is located at the transition between the Socorro Basin to the north and the San Marcial Basin to the south. Highways, the Rio Grande, the Jornada volcanic field, and stratigraphically important wells are shown for geographic reference. Psag label = outcrops of San Andres Formation limestone interbedded with Glorieta Sandstone.

2020a, 2021a). West-dipping Permian San Andres Formation and Glorieta Sandstone crop out in low hills 7 km northeast of Mesa Camp (Fig. 1). Late Eocene strata—the Baca Formation, an andesite flow, and the Spears Group—are in fault contact with Pennsylvanian and Permian bedrock units in the Little San Pascual Mountains on the western side of the range (Koning and Heizler, this volume; Koning et al., 2021a). The Baca Formation unconformably overlies the Yeso Formation, indicating that the Little San Pascual Mountains were located on the Sierra uplift indicating complete removal of the Mesozoic stratigraphy. Proximal sandstone and conglomerate deposits of the Miocene Popotosa Formation are exposed in fault slivers along the western flank of the hills. Piedmont and axial ancestral Rio Grande deposits of the early Pleistocene Sierra Ladrones Formation (both in the Santa Fe Group) lap across and are cut by faults on the west side of the Little San Pascual Mountains (Koning and Heizler, this volume).

The southern Chupadera Mountains contain ~700 m of late Eocene andesite flows, volcaniclastic sediment, and dacitic tuffs that overlie 20–40 m of the Baca Formation (Chamberlin

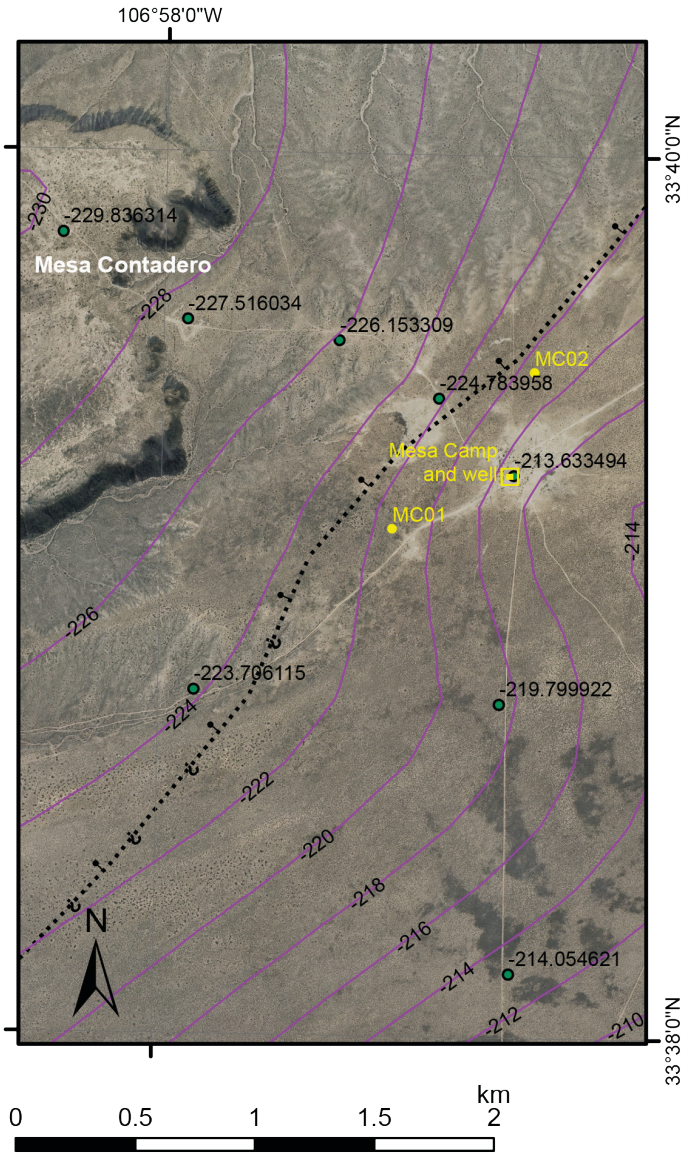

FIGURE 2. Expanded view of the study area and measured Bouguer anomaly (from Gallant et al., this volume). Purple lines are contours of the Bouguer anomaly data. The dotted (concealed) fault is drawn close to MC02 based on evidence of 3D behavior in the AMT data. This west-down, inferred fault offsets the middle of an overall northwest-dipping ramp structure (discussed in Gallant et al., this volume). The green dots are gravity stations.

and Cikoski, 2010; Koning et al., 2020a). The fact that the Baca Formation overlies Pennsylvanian strata in the southern Chupadera Mountains indicates that this area was also located on the Sierra uplift (Chamberlin and Cikoski, 2010).

A thick Mesozoic section is preserved south of Mesa Camp. Cretaceous sedimentary rocks assigned to the McRae Group crop out at the north end of the Fra Cristobal Mountains (Lucas et al., 2019; Nelson et al., 2012). A second well on the Armendaris Ranch, the Bison Corral well, located 21 km south of Mesa Camp and 13 km due east of the north end of the Fra Cristobal Mountains (33°27'41.86"N latitude, 106°57'22.59"W longitude, WGS 84; Fig. 1), was drilled to a depth of 120 m. The sequence of rock units reported on the drillers log for this well are listed in descending order, with inferred correlations listed in parentheses: 15 m of silt, clay, and sand (Santa Fe Group); 35 m of sandstone interbedded with minor gray clay and silty fine sand (Gallup Sandstone interbedded with D Cross Member of Mancos Shale); 52 m of predominantly gray-yellow clay, silt, and "oil shale" (D Cross Member of Mancos Shale); and 18 m of the partially penetrated Tres Hermanos Formation. The presence of gray-yellow clays-silts, local descriptions of "oil shale," lack of limestone beds, and lack of conglomeratic units strongly suggest this well penetrated Cretaceous strata.

Closer to Mesa Camp, stratigraphic information was gathered during the recent drilling of the Pope borehole along a gasoline-diesel pipeline 8 km south of the AMT survey site (Fig. 1). This well, which was drilled for cathodic protection of the pipeline, did not encounter groundwater. However, the drillhole did allow observations of cuttings from the axial-fluvial facies of the southward equivalent of the Sierra Ladrones Formation, the Palomas Formation of the Santa Fe Group, from the land surface to the total depth of the well (122 m). The Palomas Formation in this area generally consists of poorly cemented, well- to moderately sorted sand containing heterolithic gravel (Fig. 3). The axial-fluvial gravel is composed mainly of volcanic rock types with subordinate chert, granite, reddish siltstones, and very fine sandstones eroded from Permian strata, quartz, and quartzite (Koning et al., 2020a, 2021b). However, in the depth interval between 107 m and 116 m, the well passed through a non-axial-fluvial gravel bed that presumably was derived from local sources to the east-northeast. Most of this gravel is olive green–colored sandstone similar to that in the Crevasse Canyon Formation, a Late Cretaceous unit that overlies the Gallup Sandstone, but minor gray Paleozoic limestone is also present. The sand also has a distinctive olive-green color, presumably because of a provenance from the Crevasse Canyon Formation. The lower 6 m of the well went back into axial-fluvial sand; thus, this distinctive gravel is not part of the Baca Formation but is still part of the Santa Fe Group.

The locally derived gravel at 107–116 m in the Pope well, coupled with the subsurface stratigraphy at the Bison Corral well, indicates that the area south and southeast of Mesa Camp is underlain by Cretaceous strata that includes the Crevasse Canyon Formation. The Crevasse Canyon Formation is comprised of a lower section dominated by mudstone with minor sandstone and an upper unit that is primarily sandstone with little fine-grained material. Recently, Lucas et al. (2019) proposed the names "Flying Eagle Formation" for the lower unit and "Ash Canyon Formation" for the upper unit in the southern Fra Cristobal Mountains. The limestone clasts may have been eroded from San Andres Formation outcrops that strike NE-SW at a distance 7 km due east of Mesa Camp (Fig. 1). This belt of limestone may trend westerly in the subsurface to a point about 3 km south of the southernmost hills of the Little San Pascual Mountains.

In summary, geologic mapping indicates that Mesa Camp is underlain by several 10s to ~100 m of Sierra Ladrones Formation axial-fluvial sediment (Koning et al., 2020a). However, this cover of sand creates notable uncertainty regarding the exact bedrock stratigraphy under Mesa Camp; the interpretation

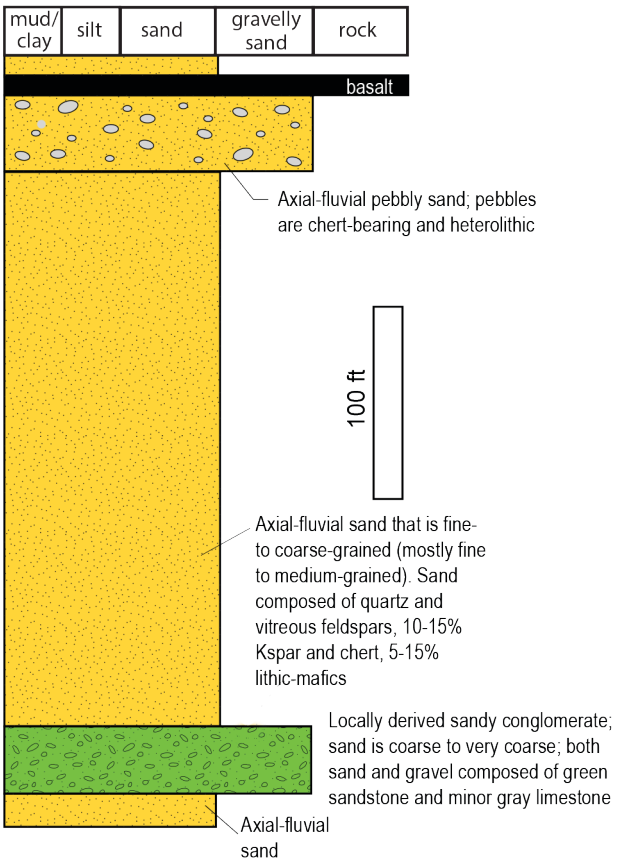

FIGURE 3. Graphic column and description of subsurface stratigraphy for the Pope borehole, drilled on January 27–28, 2022. Location is 316,945 m E, 3,717,765 m N (NAD83, zone 13). The presence of a layer of locally derived conglomerate at 107–116 m depth, composed of greenish sandstone and minor gray limestone, is interpreted to indicate the following pre–Santa Fe Group paleotopography: San Andres Formation–cored hills to the northeast (south to southwest of Little San Pascual Mountains) and pre-Laramide Cretaceous Crevasse Canyon Formation to the east. The interpreted presence of Crevasse Canyon Formation would imply that extensional strain of the Lava fault zone reactivated an earlier west-side up, west-dipping Laramide fault system, probably a northward continuation (albeit offset by younger extensional faults) of the reverse fault mapped in the northern Fra Cristobal Mountains (Nelson et al., 2012).

is highly dependent on locations of Laramide structures and uplifts relative to the site. If the site lies on the Sierra uplift, then underlying bedrock stratigraphy would probably be similar to that exposed in the Little San Pascual Mountains or the southern Chupadera Mountains (i.e., Late Eocene volcanic rocks, Baca Formation, Permian-Pennsylvanian strata). On the other hand, if the site lies outside of the uplift, a thick Cretaceous section would be expected to underlie the Sierra Ladrones Formation.

Field Parameters

The Mesa Camp water well, located about 1 km from each AMT site, has a static water level that was measured in March 2022 at 84 m below land surface, and the bottom of the well is 94 m below land surface. Field parameters were measured while the well was pumped at 3 gpm. The well went dry after 10 minutes (30 gallons). The field parameters, especially temperature, were relatively stable in the last 4 minutes of pumping. The temperature was 19.92°C, the conductivity was 1923 µS/cm (range of 1923–1933), the total dissolved solids (TDS) was 1250 mg/L (range of 1250–1258), and the pH was 8.2. The water in the well is sufficiently salty as to be unpalatable.

AUDIO-MAGNETOTELLURIC SURVEY NEAR MESA CAMP

Resistivity of Subsurface Rocks and Fluids

The AMT geophysical method measures subsurface electrical resistivity, which is affected by physical properties including rock type, porosity and its connectivity, water content, and groundwater salinity (Fig. 4). Saline water, clays, and mineralized rocks all conduct electric currents well (i.e., are conductive), whereas water with TDS <1000, anhydrite, and unaltered bedrock with little permeability or porosity are poor conductors of electrical currents (i.e., are resistive). Consequently, AMT data can provide information about the hydrogeologic character of the local sedimentary rocks in the subsurface near the Mesa Camp well. Sedimentary rocks containing saline pore fluids can have bulk formation resistivity of <10 Ohm-m (Fig. 4) based on Archie's law:

$$\sigma = \sigma_{fluid} \phi^m$$

where σ is bulk electrical conductivity, σ_{fluid} is fluid electrical conductivity, ϕ is porosity, and m is a cementation factor that is related to the connectivity of the pores (Archie, 1942). Formation resistivity (ρ) is the inverse of electrical conductivity ($\rho = 1/\sigma$). Sand with freshwater in the pores can have resistivity values >100 ohm-m (Fig. 4). The axial-fluvial facies of the Santa Fe Group is primarily composed of clean sand.

Methods

The AMT technique utilizes naturally occurring electromagnetic waves generated by lightning (high frequency) and interaction of solar winds with the Earth's magnetosphere (low frequency; Simpson and Bahr, 2005). These natural magnetic field variations induce eddy currents in the Earth's crust that can be measured at the surface to better understand subsurface electrical resistivity. Low frequency (long period) signals penetrate deeper than high frequency (short period) waves. Therefore, measuring signals over a large frequency range can provide resistivity information to depths from a few 10s of meters to >1 km. The AMT field setup uses induction coils to measure the Earth's magnetic field as a function of time, and an array of electrodes captures subsurface electrical responses to magnetic field variations over time. Because the electric (E) and the magnetic (H) fields are measured in orthogonal directions, the data have four components that are generally presented in the form of the impedance tensor, Z (Chave and Jones, 2012), which has both real and imaginary terms. The real component is used to calculate apparent resistivity curves as a function of

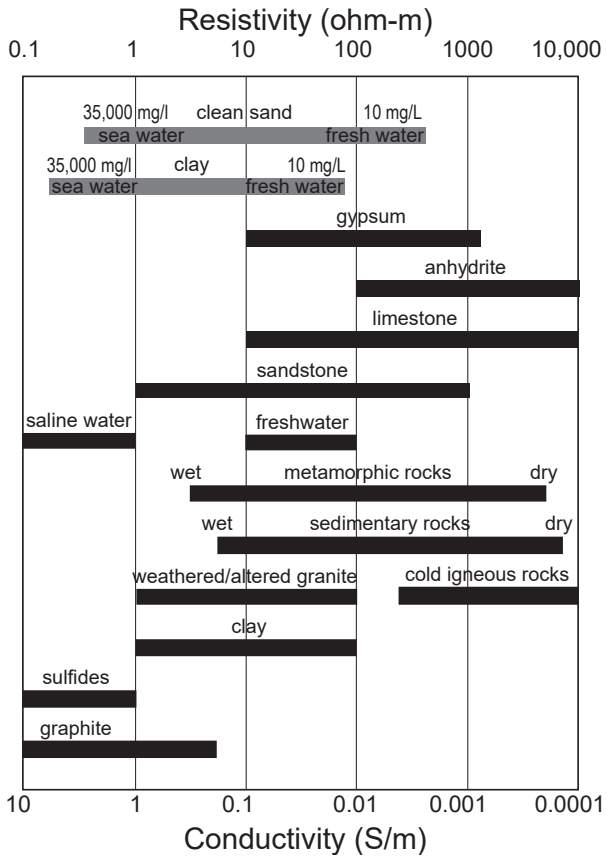

FIGURE 4. Black bars illustrate the range of electrical conductivities (or resistivities) of common subsurface materials (after Lowrie, 2007; Guinea et al., 2012; Peacock et al., 2015; Caselle et al., 2019). Wet and dry refers to pores or fractures that are filled with water or air. The gray bars represent end member formation resistivity conditions for fresh (10 mg/l) and seawater (35,000 mg/l) in clean sand and in clay using a cementation factor of 2 and porosity of 0.3 in Archie's Law.

period/frequency; apparent resistivity is the average resistivity of the subsurface in a uniform half-space (Simpson and Bahr, 2005). The imaginary terms are used to derive the phase, which is similar to the gradient of apparent resistivity and is diagnostic of resistivity stratification (Simpson and Bahr, 2005). The data are measured in the time domain, but are converted to the frequency domain using Fourier transform methods. Apparent resistivity and the phase are plotted as a function of period and are modeled together to estimate the subsurface resistivity structure using inversion methods.

In our study, we collected AMT data using a Zonge GDP32-24 data logger and Zonge ANT-6 induction coils that work in the frequency range of 0.1–10,240 Hz to measure horizontal magnetic fields. The induction coils were buried in shallow (about 0.3–0.4 m) trenches. Electric fields were measured using an L-shaped electrode array with 40 m dipoles and three silver–silver chloride SRE-011-SPB electrodes buried in small holes with bentonite and salty water (Fig. 5). The electrical array and induction coils were oriented north-south and east-west using magnetic north. Data were collected using a variable sample-rate time schedule of 192–8192 Hz (period: 5.2E-3–1.2E-4 s) for 2 minutes, 3–256 Hz (3.3E-1–3.9E-3 s) for 10 minutes, and .0938–8 Hz (10.7–0.125 s) for 20 min-

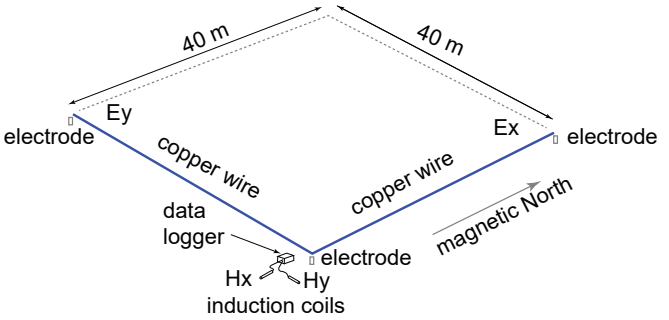

FIGURE 5. Field setup for AMT.

utes, which allowed for sampling of the AMT response across a wide frequency range to attain resistivity information at a series of depths. The data were analyzed in the field by first assessing the time series for quality, then applying a Fourier transform to the data and evaluating the resulting spectra, and then calculating apparent resistivity and phase curves by using Zonge software (MacInness, 2010, 2014). If the curves were complete and relatively free of noise, the equipment was moved to a new station.

Once back in the office, the quality of the data was improved by removing low-coherence data and obvious man-made noise. EM-community-standard .EDI files were created using Zonge software, which were then imported into the computer program WinGLink to make static shift corrections; static shift is caused by distortion arising from near-surface conditions that can sometimes affect the signal measured by the electrodes, which causes a uniform shift of the apparent resistivity curves to higher or lower values (Pellerin and Hohmann, 1990; Chave and Jones, 2012). WinGLink was also used to create one-dimensional (1D) resistivity inversion models and cross-sectional diagrams based on the 1D models.

MTpy (Krieger and Peacock, 2014) was used to calculate phase tensors in order to assess the dimensionality of the resistivity structure in the subsurface. Phase tensors are described in detail in Caldwell et al. (2004) and Bibby et al. (2005). Plots of phase tensors and ellipticity are commonly used to evaluate and visualize this dimensionality (Fig. 6; Caldwell et al., 2004; Bibby et al., 2005; Booker, 2014). Phase tensors are plotted graphically as circles or ellipses by comparing principal axes of the tensor. Circles represent 1D structure, slightly skewed ellipses represent 2D structure, and strongly skewed elliptical shapes represent 3D structure. In addition to providing insight into the complexity of the subsurface, dimensionality helps determine the appropriate inverse modeling scheme.

Results

Figures 6 and 7 show the apparent resistivity, phase, and phase tensors for each station after low-coherence data and anthropogenic noise were removed from the data. The data for site MC01 indicate 1D resistivity structure. In contrast, 2D and 3D effects in the shallow subsurface, which likely are related to cultural noise, impacted the AMT data collected at site MC02. MC02 is near the southward projection of the east strand of

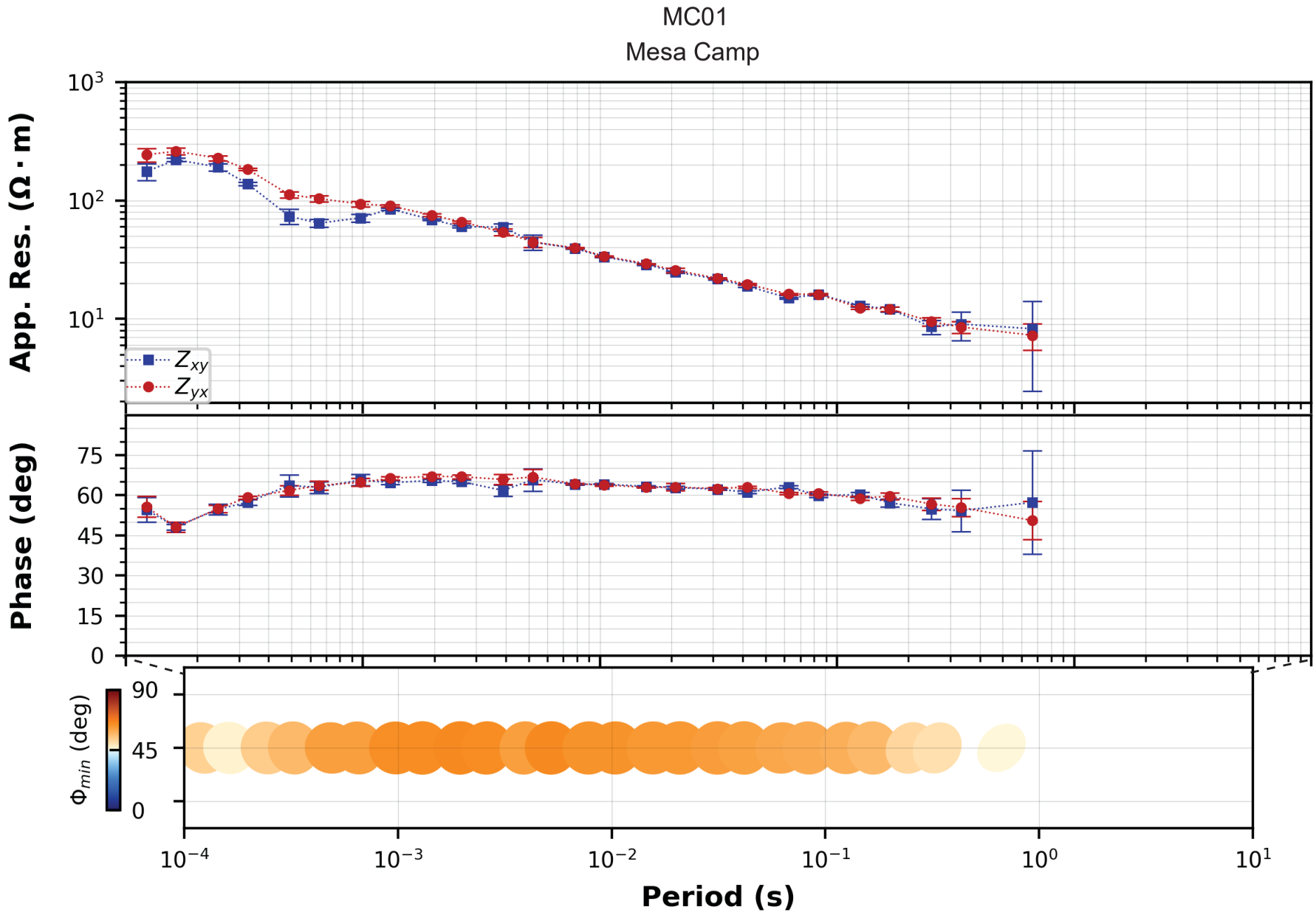

FIGURE 6. Upper Panel: Apparent resistivity (App. Res.) and phase versus period for MC01. The apparent resistivity curve displays a small static shift of <20 ohm-m. The x-axis for the upper panel is depicted at the bottom of the lower panel but is expanded as illustrated by the dashed lines. Lower Panel: The phase tensor and color-coded skew angle data (note scale at left) for this site indicate 1D structure. The deepest three points (to the right) were removed prior to modeling because of their high uncertainty.

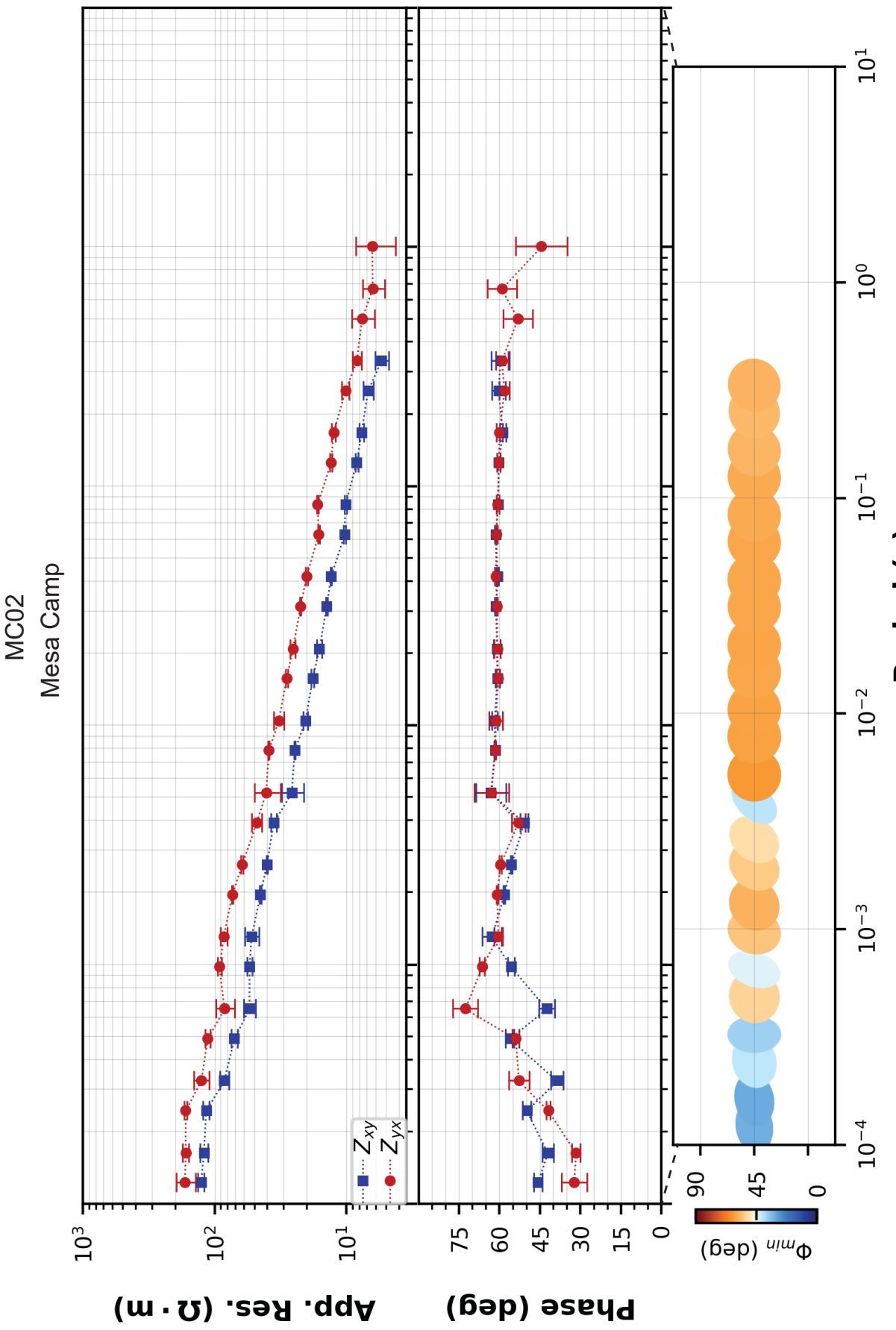

FIGURE 7. Upper Panel: Apparent resistivity (App. Res.) and phase versus period for MC02. The apparent resistivity curve displays a static shift of 50 ohm-m. The x-axis for the upper panel is depicted at the bottom of the lower panel, but is expanded as illustrated by the dashed lines. Lower Panel: The phase tensor and color-coded skew angle (note scale at left) data for this site indicate shallow 2D and 3D structure, which may be affected by cultural noise, and deep 1D structure. The deepest three points with relatively large error bars were removed prior to modeling.

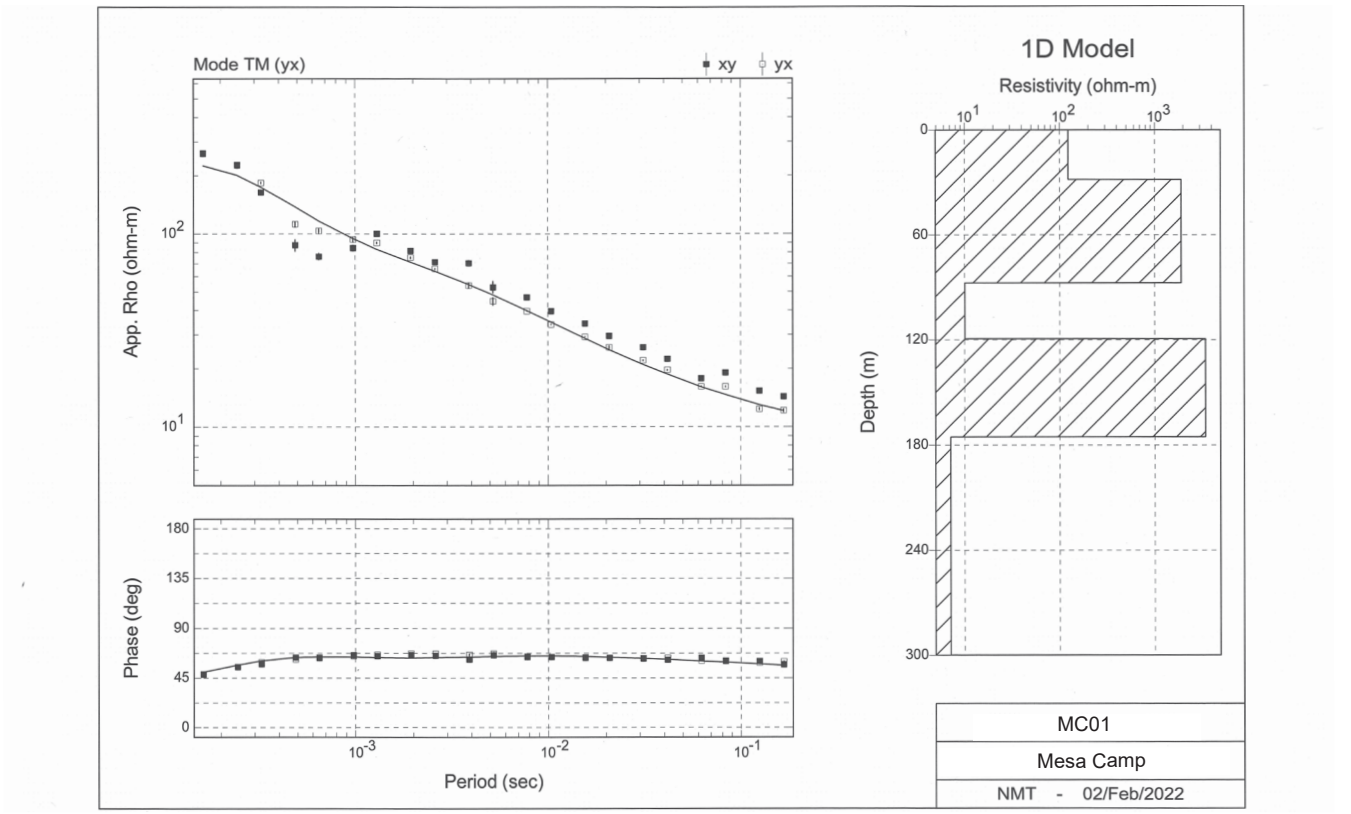

FIGURE 8. Apparent resistivity and phase versus period plots and the 1D model that best fits the TM mode apparent resistivity (App. Rho) data (open symbols) for site MC01.

the Little San Pascual Mountain fault. Because the modeling software is based on a 1D assumption, all 3D points identified in the analysis of the data from MC01 were removed prior to inversion, and 2D points were retained in this preliminary evaluation of the data. The inversion for MC01 was run in the TM mode, which is common practice for minimizing multi-dimensional effects (Wannamaker et al., 1984). Because cultural noise may be affecting the highest frequency data from MC02, the invariant mode, which averages the TE and TM modes, is used to smooth out this noisy dataset.

Examination of Figures 6 and 7 reveals that the apparent resistivity curves for both sites are affected by static shift. Commonly, the transient electromagnetic (TEM) method is used to correct for static shift, since this method does not rely on electrodes to estimate resistivity structure (Pellerin and Hohmann, 1990). The TEM method is a time-domain, surface-based geophysical technique that measures the electrical resistivity of the subsurface using an applied current. TEM data is used to help decide whether to shift the curves up or down. We did not collect TEM data as part of this study. Instead, we ran the 1D inversion models twice, once shifting the blue YX curve up, and once shifting the red XY curve down; this approach makes the simplifying assumption that both curves have not been static shifted. Overall, the former shift (blue up) does not affect the shape of the model result, and the latter shift (red down) has the effect of decreasing resistivity across the entire depth of investigation by <50 ohm-m in the case of MC02.

The WinGLink 1D inversion model was run several times to test the robustness of the results. A simple examination of the apparent resistivity curves (Figs. 8–9) shows that a lower conductivity interval (i.e., a dip in the curve) is present at shallow depth in both datasets; the dip in the curve is smaller in MC02. If the 3D data from MC02 are removed, that lower conductivity interval disappears. If the shallow 3D data are left in, and if the data for MC02 are modeled in the invariant mode, the 1D models for both MC01 and MC02 have similar shapes. In the case of MC01 (Fig. 8), the model indicates a resistive layer to a depth of about 90 m, a conductive layer between 90 m and 120 m, a second resistive layer between 120 m and 175 m, and conductive material below 175 m. Among the various model runs, the top of the shallow conductor is at depths of 78–101 m, the base is at 108–128 m, and the thickness is between 7 m and 44 m (average 26 m). The top of the deeper conductive layer is at depths of 158–175 m. As is common with this type of modeling, the depth and thickness results are non-unique, but the existence of the shallow conductor at the MC01 site appears to be a real feature. The invariant model for MC02 produces a 1D model that is characterized by resistive rocks in the upper 70–80 m (Fig. 9), a conductive layer with a base at 100–120 m, and a resistive layer with a base at 160–175 m. Note that the resistivity of the upper "conductive" layer for MC02 is 15 ohm-m, compared to 8–10 ohm-m for MC02, consistent with the magnitude of the dip described earlier in the qualitative discussion of the apparent resistivity curves.

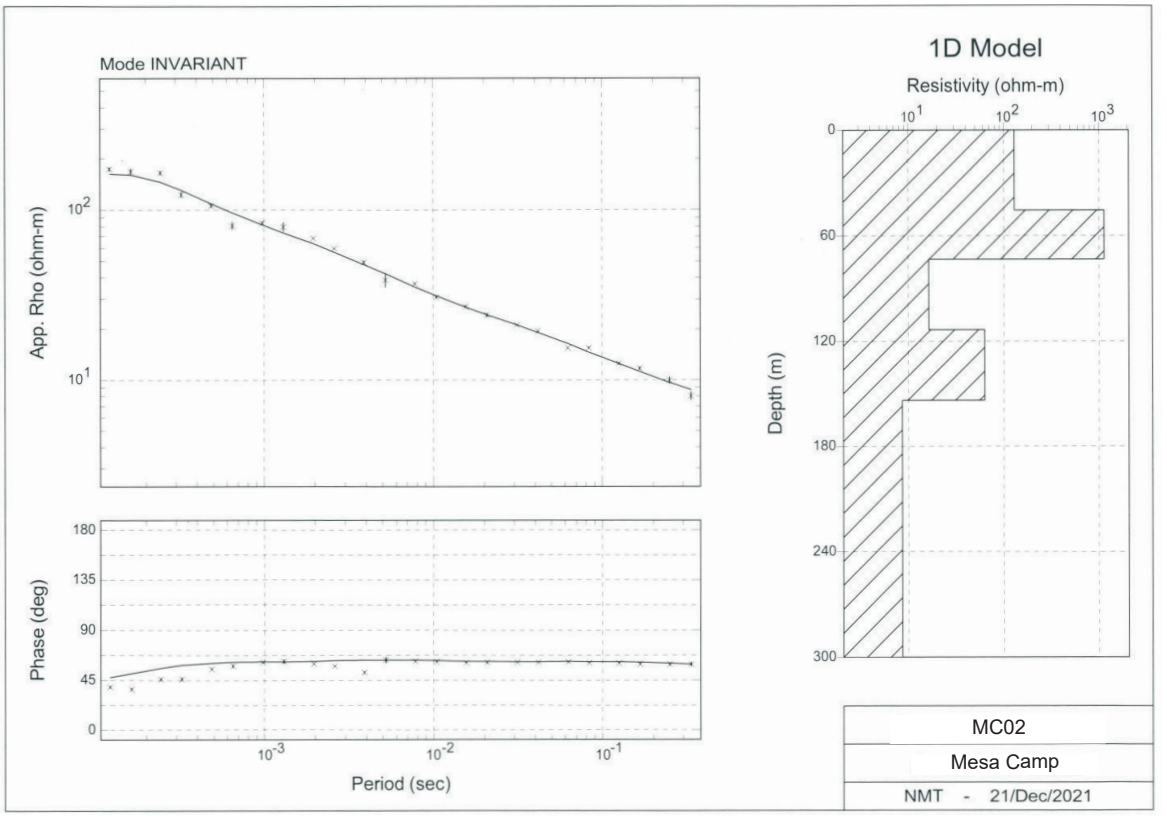

FIGURE 9. Apparent resistivity and phase versus period plots and a 1D model that best fits the invarient mode apparent resistivity (App. Rho) data for site MC02.

DISCUSSION AND SUMMARY

The AMT data are combined with lithologic information derived from the nearby Pope well, the distant Bison Corral well, and the geologic mapping of Koning et al. (2020a, 2021b) to infer the subsurface hydrogeology of the Mesa Camp area. The upper resistive interval at both sites (MC01 and MC02) likely corresponds to the vadose zone in Sierra Ladrones Formation axial-fluvial sand. This correlates nicely with the depth-to-water reported for the Camp Mesa well at ~84 m. This study demonstrates that the AMT method is capable of detecting the base of the vadose zone in this area.

The interpretation of the conductive and resistive intervals that lie below 70–80 m is more speculative. Based on the observations from the Pope well, the Sierra Ladrones (Palomas) axial-fluvial facies does contain layers of piedmont gravel, and based on observations in other areas, this unit also contains muddy floodplain deposits. However, the muddy floodplain deposits were <3–6 m thick in the Pope well and are typically <6 m thick in axial-fluvial sediment along the Rio Grande. For example, the axial-fluvial facies is sandy and lacks clays in the 85 m thick section locally exposed under Mesa del Contadero (Koning et al., 2020a).

Three geologically reasonable options for the interpretation of the shallow conductive, deeper resistive and deep conductive intervals are illustrated in Figure 10. The first interpretation is based on local rock units exposed in the Little San Pascual Mountains to the northeast. In this scenario, the shallow conductive unit is interpreted to be a clay-rich distal basin-floor facies of the Popotosa Formation, which unconformably overlies resistive Glorieta Sandstone and San Andres Formation limestone that conformably overlies clayey sandstone in the Los Vallos Formation in the Yeso Group. The Los Vallos sandstone may be saturated with brackish water. The San Andres Formation limestone in the southernmost Little San Pascual Mountains is silicified, and that silicification potentially projects into the Mesa Camp area.

The second scenario predicts that the lower resistor is composed of indurated, late Eocene volcanic and volcaniclastic strata that overlies conglomeratic Baca Formation. An unconformity exists between the Baca Formation and the lowest conductor. The lowest conductor consists of the Abo Formation or, similar to the first scenario, Los Vallos Formation saturated with salty groundwater that overlies the Abo Formation.

The third scenario is based on the interpretation of the piedmont gravel interval in the Pope well and the interpretation of the drillers log for the Bison Corral well. In this case, Cretaceous sedimentary rocks underlie Mesa Camp. The shallow conductive interval is the fine-grained lower part of the Crevasse Canyon Formation (the Flying Eagle Formation of Lucas et al., 2019), consistent with the erosion of the sandy upper part of the Crevasse Canyon Formation (Ash Canyon Member of Bushnell, 1955) based on the olive-green sandstone clasts observed in the piedmont gravels in the Pope well. The resistive layer is assigned to the Gallup Sandstone, a tight fine-grained sandstone, and the deep conductive layer is assigned to the D Cross Tongue of the Mancos Shale, based on the analysis of the Bison Pasture well.

Given the general similarity in the shape of the apparent resistivity curves and the 1D models, significant structure is not present between sites that are located <1 km from each other, consistent with the gravity observations of Gallant et al. (this volume). The 3D AMT data at shallow depth in MC02 possibly could indicate the presence of a nearby fault, if cultural noise is not the culprit. Therefore, we tentatively draw the southern extension of the west strand of the Little San Pascual Mountain

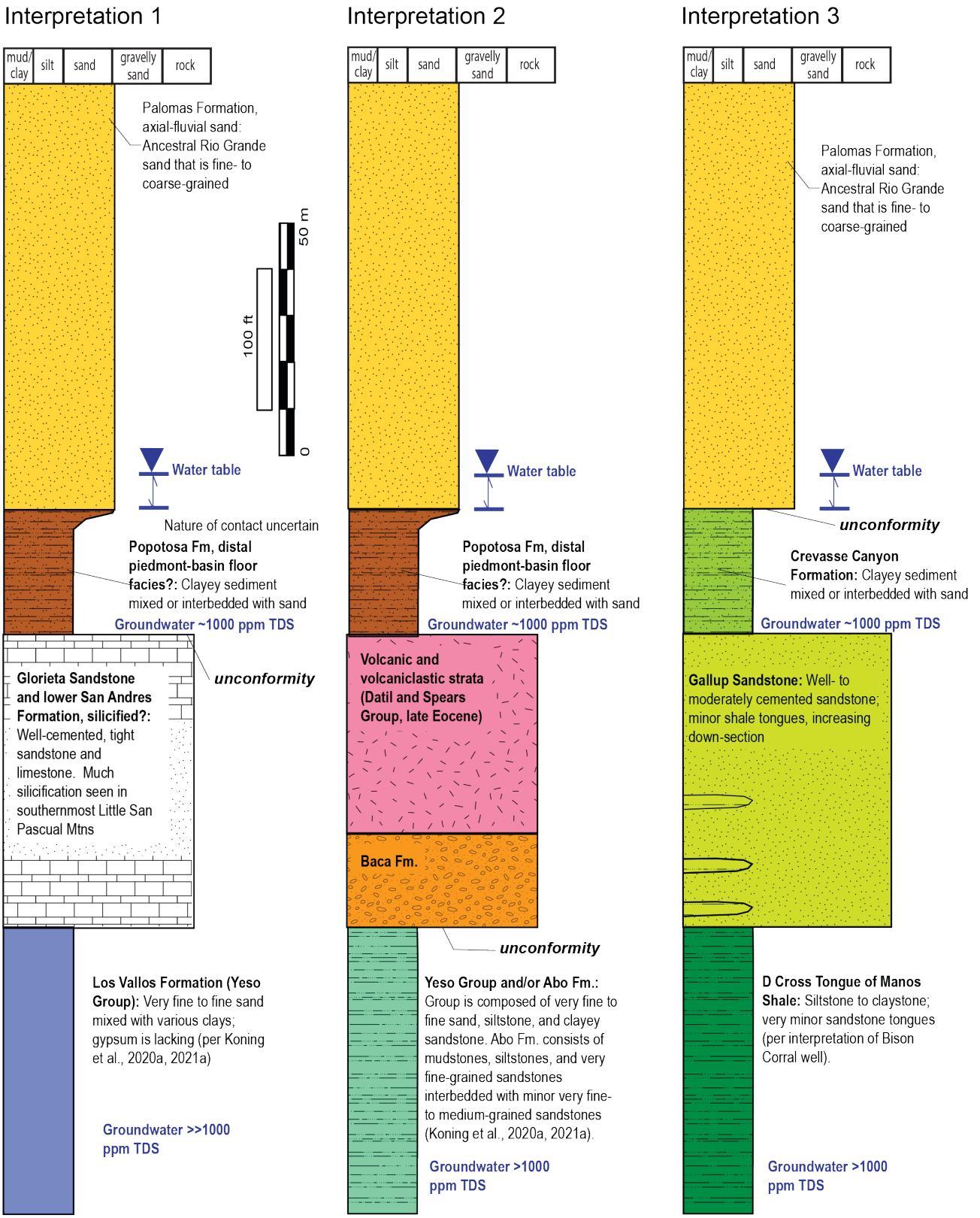

FIGURE 10.Three possible geologic interpretations of the resisitive-conductive-resistive-conductive intervals measured during the AMT survey near Mesa Camp.

fault to within 100 m of MC02, but since there is little 3D behavior in MC01, the fault is drawn >100 m to the north of that measurement site.

In summary, this pilot AMT investigation did provide useful information about the hydrogeology of the subsurface. Most importantly, the depth to the base of the resistive vadose zone is consistent with depth to water measured in the Mesa Camp well. The alternative interpretations of the hydrogeologic units associated with the deeper intervals imaged by AMT can be tested either by drilling or by using other geophysical techniques. Which interpretation proves to be correct would have notable implications regarding the location of buried, major Laramide structures. Additional AMT surveys in the vicinity of wells with drillers logs or cuttings in this region (e.g., the Bison Corral) would also be useful in testing the analysis presented here.

ACKNOWLEDGMENTS

We thank Marissa Frichera and Kyle Gallant for their assistance with the fieldwork. Gravity data in Figure 2 was shared by Kyle Gallant and Alex Rinehart and is from their paper in this volume. We thank the Armendaris Ranch for permission to access the field sites. We express gratitude to Jeff Pepin and Mark Person for their careful and constructive reviews that greatly improved the manuscript.

REFERENCES

Archie, G.E., 1942, The electrical resistivity log as an aid in determining some reservoir characteristics: Transactions of the AIME, v. 146, 9 p.

Bibby, H.M., Caldwell, T.G., and Brown, C., 2005, Determinable and non-determinable parameters of galvanic distortion in magnetotellurics: Geophysical Journal International, v. 163, p. 915–930, https://doi.org/10.1111/j.1365-246X.2005.02779.x.

Booker, J.R., 2014, The magnetotelluric phase tensor: A critical review: Survey of Geophysics, v. 35, p. 7−40.

Bushnell, H.P., 1955, Mesozoic stratigraphy of south-central New Mexico: New Mexico Geological Society, Guidebook 6, p. 81–87.

Caldwell, T.G., Bibby, H.M., and Brown, C., 2004, The magnetotelluric phase tensor: Geophysical Journal International, v. 158, p. 457−469.

Caselle, C., Bonetto, S., and Comina, C., 2019, Comparison of laboratory and field electrical resistivity measurements of a gypsum rock for mining prospection applications: International Journal of Mining Science and Technology, v. 29, p. 841–849, doi.org/10.1016/j.ijmst.2019.09.002.

Cather, S.M., 1983, Laramide Sierra uplift: Evidence for major pre-rift uplift in central and southern New Mexico: New Mexico Geological Society, Guidebook 34, p. 99–101.

Chamberlin, R.M., and Cikoski, C.T., 2010, Geologic map of the Indian Well Wildnerness Quadrangle, Socorro County, New Mexico: New Mexico Bureau of Geology and Mineral Resources, Open-file Geologic Map OF-GM-201, scale 1:24,000.

Chave, A., and Jones, A., 2012, The Magnetotelluric Method: Theory and Practice: Cambridge, United Kingdom, Cambridge University Press, 570 p.

Gallant, K., Koning, D.J., and Rinehart, A., this volume, Elucidating the structural geometry of the San Marcial Basin, Sierra County, using terrain-corrected Bouguer anomaly gravity data: New Mexico Geological Society, Guidebook 72.

Guinea, A., Elisabet, P., Lluís, R., Juan, J.L., and Pilar, Q., 2012, The electrical properties of calcium sulfate rocks from decametric to micrometric scale: Journal of Applied Geophysics, v. 85, p. 80–91.

Jochems, A.P., and Love, D.W., compilers, 2016, Fault number 1995, Little San Pasqual fault, in Quaternary fault and fold database of the United States: U.S. Geological Survey website, https://earthquakes.usgs.gov/hazards/qfaults (accessed 04/14/2022).

Koning, D.J., and Heizler, M.T., this volume, Stratigraphy and sedimentology of the Santa Fe Group adjoining the Little San Pascual Mountains—implications for footwall exhumation and evolution of the Little San Pascual Mountain fault system: New Mexico Geological Society, Guidebook 72.

Koning, D.J., Pearthree, K.S., Jochems, A.P., and Love, D.W., 2020a, Geologic map of the San Marcial 7.5-minute quadrangle, Socorro County, New Mexico: New Mexico Bureau of Geology and Mineral Resources, Open-file Geologic Map 287, scale 1:24,000.

Koning, D.J., Jochems, A.P., Hobbs, K.M., Pearthree, K.S., and Love, D.W., 2020b, Geologic map of the Paraje Well 7.5-minute quadrangle, Socorro County, New Mexico: New Mexico Bureau of Geology and Mineral Resources, Open-file Geologic Map 286, scale 1:24,000.

Koning, D.J., Nelson, W.J., and Elrick, S., 2021a, Geologic map of the Little San Pascual Mountain 7.5-minute quadrangle, Socorro County, New Mexico: New Mexico Bureau of Geology and Mineral Resources, Open-file Geologic Map 296, scale 1:24,000.

Koning, D.J., Hobbs, K.M., Pearthree, K.S., and Love, D.W., 2021b, Geologic map of the Fort Craig 7.5-minute quadrangle, Socorro County, New Mexico: New Mexico Bureau of Geology and Mineral Resources, Open-file Geologic Map 288, scale 1:24,000.

Koning, D.J., Chamberlin, R., and Love, D.W., this volume, Chupadera Mountains, Second-day road log, from Socorro to Box Canyon, northern Chupadera Mountains, Nogal Canyon, and San Antonio: New Mexico Geological Society, Guidebook 72.

Krieger, L., and Peacock, J.R., 2014, MTpy: A Python toolbox for magnetotellurics: Computers and Geosciences, v. 72, p. 167−175.

Lowrie, W., 2007, Fundamentals of Geophysics: New York, Cambridge University Press, 393 p.

Lucas, S.G., Nelson, W.J., Krainer, K., and Elrick, S.D., 2019, The Cretaceous system in central Sierra County, New Mexico: New Mexico Geology, v. 41, p. 3–39.

MacInnes, S., 2010, MTEdit Documentation: Tucson, AZ, Zonge Engineering and Research Organization, 14 p.

MacInnes, S., 2014, MTFT24 Documentation: Tucson, AZ, Zonge Engineering and Research Organization, 23 p.

Nelson, W.J., Lucas, S.G., Krainer, K., McLemore, V., and Elrick, S.D., 2012, Geology of the Fra Cristobal Mountains, New Mexico: New Mexico Geological Society, Guidebook 63, p. 195–210.

Peacock, J.R., Mangan, M.T., McPhee, D., Ponce, D.A., 2015, Imaging the magmatic system of Mono Basin, California, with magnetotellurics in three dimensions: Journal of Geophysical Research Solid Earth, v. 120, p. 7273–7289, https://doi.org/10.1002/2015JB012071.

Pellerin, L., and Hohmann, G.W., 1990, Transient electromagnetic inversion: A remedy for magnetotelluric static shifts: Geophysics, v. 55, p. 1242−1250.

Simpson F., and Bahr, K., 2005, Practical Magnetotellurics: Cambridge, United Kingdom, Cambridge University Press, 254 p.

Wannamaker, P.E., Hohmann, G.W., and Ward, S.H., 1984, Magnetotelluic responses of three-dimensional bodies in layered earths: Geophysics, v. 49, p. 1517–1533.

The iconic denizen of the American Southwest. Photo by Scott Elrick.